ISSN 0001-4370, Oceanology, 2021, Vol. 61, No. 4, pp. 569–580. © Pleiades Publishing, Inc., 2021.
Russian Text © The Author(s), 2021, published in Okeanologiya, 2021, Vol. 61, No. 4, pp. 649–661.

INSTRUMENTS AND METHODS

Underwater Acoustic Communications Using Vertical Receiver Arrays in Ice-Covered Shallow-Water Areas

M. V. Volkov[a], A. A. Lunkov[a, b], V. G. Petnikov[a, *], and A. V. Shatravin[a, c, **]

[a] *Prokhorov General Physics Institute, Russian Academy of Sciences, Moscow, 119991 Russia*
[b] *Bauman Moscow State Technical University, Moscow, 105005 Russia*
[c] *Shirshov Institute of Oceanology, Russian Academy of Sciences, Moscow, 117997 Russia*
**e-mail: petniko@kapella.gpi.ru*
***e-mail: ashatravin@ocean.ru*

Received August 1, 2020; revised November 30, 2020; accepted February 14, 2021

Abstract—The feasibility of underwater acoustic communications in an ice-covered shallow-water area is demonstrated in a field experiment and by computer modeling. The advantages of vertical linear receiver arrays with different lengths and different numbers of hydrophones are investigated. The study analyzes the case when the water area depth is much smaller than the distance to the receiver array. A comparative analysis of several algorithms of spatial signal processing for binary phase-shift keyed signals with a carrier frequency of about 1 kHz at different information transmission rates is carried out. The experiment was conducted on Lake Baikal with an ice cover thickness ≈66 cm and under intense acoustic noise associated with crack formation in the ice surface. It is shown that when a vertical array is used, the bit error rate can be reduced by more than three times versus a single receiver.

Keywords: underwater acoustic communications, vertical hydroacoustic arrays, sound propagation in ice-covered shallow-water areas

DOI: 10.1134/S0001437021040160

INTRODUCTION

Industrial development and environmental monitoring of the ocean shelf and inland waterbodies require new technologies for communication with autonomous underwater vehicles of various design. For ice-covered water areas, such in-demand and nonalternative technologies include underwater acoustic communications (UAC) (see, e.g., [5, 10], which describe the results of using standard UAC modems with single sound sources and receivers in the Arctic Basin). It is also known that, in general, in shallow-water areas, vertical receiver arrays make it possible to significantly improve the quality of UAC [1, 2, 8, 15]. It turns out to be possible even without traditional signal processing algorithms for this type of communication [7, 11, 16] and is associated with the fact that vertical arrays suppress both types of interference arising in the case of UAC, i.e., intersymbol interference and background acoustic noise. However, in complex and variable sound propagation conditions with ice cover and strong natural acoustic noises, the improvement in UAC provided by the array is quite difficult to predict. Experimental results that make it possible to estimate such improvement are clearly insufficient, and the assumptions in UAC problems based on the general theory of digital communication are often untenable [14]. This is, first, due to the fact that the ice cover in natural water areas cannot be considered as a single ice mass of constant thickness. In field conditions, ice is covered with cracks, and its lower boundary is a hard surface with characteristic roughness (see, e.g., [9]). All this leads to the fact that the spatial fields of ice parameters, including the sound speed fields of longitudinal and transverse waves, and the fields of the attenuation coefficients of these waves are random, and also time-dependent. Roughness and cracks on ice change their properties and even reappear. The ice concentration can also be significantly less than ten when the ice cover alternates with large ice leads, as, for example, was the case in the experiments described in [1]. Second, crack formation can generate rather intense and nonstationary acoustic noise.

In this article, experimental estimations of the UAC characteristics on Lake Baikal in winter are presented. The aim of this work is to find the advantages of using vertical linear receiver arrays for the specified type of communication under continuous ice cover (ice concentration is close to ten). It is shown that the use of autonomous vertical arrays lowered to the bottom from the shore-fast ice (ice frozen to the shore) ensures stationary array placement and the possibility of long-term stable communication in the frequency

range close to 1 kHz. In a sense, this range is optimal for the shallow Arctic shelf and, first of all, for the areas with sound speed in the bottom less than the sound speed in the water [2]. Such Arctic regions are characterized by increased attenuation of acoustic waves propagating in the water layer.

When using vertical linear arrays consisting of chains with equidistant hydrophones, the important parameters are the necessary number of these receivers and the ratio of the array length to the depth of the water area in the place of its use. The smaller the absolute value of the specified parameters, the lower the cost of such an array and the longer its autonomous operation time determined by the power consumption of hydrophone preamplifiers and the primary information processing unit can be. It follows from [8] that the array remains effective even when the distance between hydrophones is much greater than half the sound wave length λ corresponding to the carrier frequency of acoustic signals. The following numerical simulation demonstrates this efficiency for different combinations of the number of hydrophones, the distances between them, and the array length, respectively. The main focus is on the efficiency of spatial processing at small distances ($r \approx 2H - 40H$, H is the water depth) between the sound source and the array, when the sound field in the hydroacoustic channel is described by a large number of energy-carrying waveguide modes, including both propagating and leaky modes. In this case, the intersymbol interference is the strongest, and this situation usually takes place in the case of UACs with autonomous underwater vehicles which have low-power sound sources.

EXPERIMENTAL STUDIES OF UNDERWATER ACOUSTIC COMMUNICATIONS

Experiments on underwater acoustic communications were carried out in the shallow part of Lake Baikal, where an autonomous vertical chain of $J = 10$ hydrophones was installed at a depth of $H \approx 41$ m in March 2019 (Fig. 1a). The chain was lowered from the shorefast ice typical of Baikal at this time of year. Digitization and recording of received signals $p_j(t)$ in the flash-memory were carried out using an information processing unit in a special sealed container, which also has batteries for powering the hydrophone preamplifiers. The container was located on the ice surface. The carrying cable of the hydrophone chain was stretched between the bottom anchor and the anchor on the ice surface, which ensured the stationary position of the receiving hydrophones at the corresponding depths z_j:

$$z_j = 0.64 + (j-1)\times 3.5 \text{ m}, \quad (1)$$

where $j = 1,\ldots,J$ is the number of the receiving hydrophone. Depths here and below are counted from the water–ice interface. Ice cover thickness was $h = 0.66$ m. The dependence of sound speed on depth at the place of the experiment calculated from the results of measurements of the vertical temperature profile is shown in Fig. 1b. It can be seen that the sound speed varied insignificantly with depth.[1]

UAC data transmission was carried out using a remote sound source (transducer) located at a distance of $r = 353$ m from the receiving array. The source was attached to a carrying halyard stretched between the bottom and the ice cover. The source was at a depth of $z_0 = 18.4$ m, and the transducer installation point was at a depth of $H = 55$ m. The acoustic track (source – receiver array) was oriented approximately parallel to the shoreline (Fig. 2). The experimental conditions are described in more detail in [3].

The transmitted binary signal $s_0(t)$ (range of values +1 and –1) included a preamble of two M-sequences, a random sequence of 2000 symbols, and a postamble also as an M-sequence. M-sequences with different numbers of symbols from 127 to 1023 were used for the preamble and postamble. The emitted signal $\hat{s}_0(t)$ was generated by modulating a carrier signal with a frequency of $f_c = 735$ Hz from the signal $s_0(t)$ prefiltered through a root raised cosine filter. The filtering makes it possible to obtain a flatter frequency response and concentration of the power of the transmitted signal in the operating frequency band compared to the ordinary binary phase shift keying [12]. The data rate for different signals was $q = 122.5$ or 183.75 bps (6 or 4 carrier periods per symbol).

Standard algorithms were used to process the received signals, as shown in Fig. 3. Quality of UAC data transmission was estimated by means of the bit error rate (BER) equal to the ratio of erroneous bits (symbols) to the total number of bits of transmitted data, and the signal to noise-plus-interference ratio (SNIR) calculated for the so-called "soft output" of decoding by the following formula:

$$\text{SNIR} = 20\log_{10}\left(\frac{\sqrt{N}}{\sqrt{\sum_n \left|K_j y_j(n) - s_0(n)\right|^2}}\right), \quad (2)$$

where $N = 2000$ is the number of symbols in the transmitted binary sequence $s_0(n)$, $y_j(n)$ is the complex demodulated signal received at a hydrophone j and digitized with frequency one sample per symbol (see Fig. 3a), and K_j is the normalization factor calculated by the following formula

[1] Additional calculations showed that these small variations in sound speed had almost no effect on the general UAC patterns noted in this article.

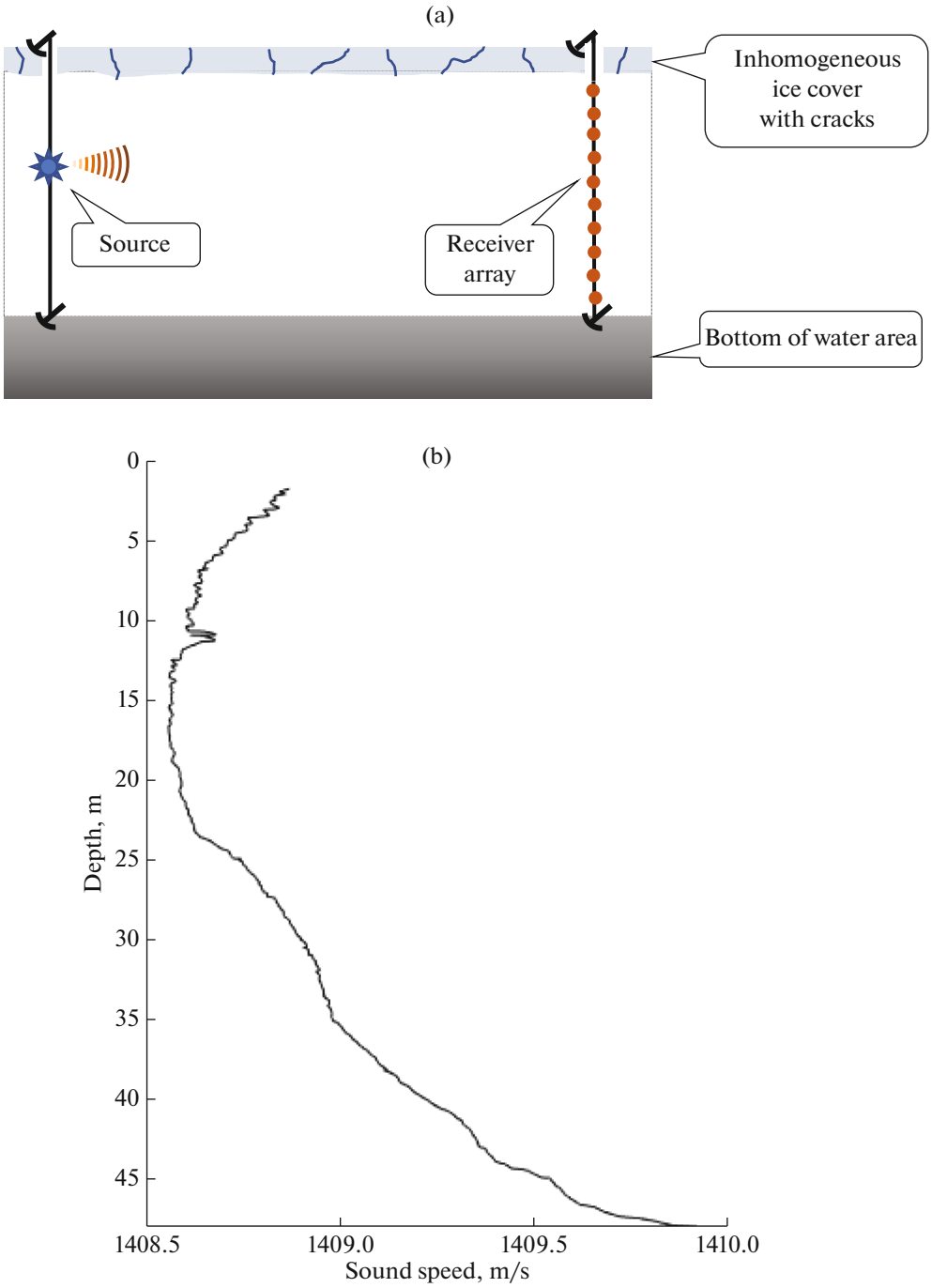

Fig. 1. Underwater acoustic communication experiment in Lake Baikal in March 2019: (a) scheme of experiment and (b) dependence of sound speed in water on depth calculated from vertical temperature profile measurements.

$$K_j = \frac{N}{\max\limits_k \left| \sum\limits_n y_j(n-k)\, s_0(n) \right|}. \qquad (3)$$

Such normalization corresponds to reduction of the maximum by amplitude arrival level in the pulse response to unity and makes it possible to estimate the noise-plus-interference level as a difference between the values of the soft output and the original binary sequence. The normalization does not affect the final result of decoding and serves only for the estimation of the total contribution of the intersymbol interference and additive noise to the received signal. In Table 1, the obtained values of SNIR and BER for single hydrophones averaged on four communication signals and also for a coherent sum of four signals are given. Note that at the obtained SNIR values the low communication quality is quite expected. Figure 4a shows

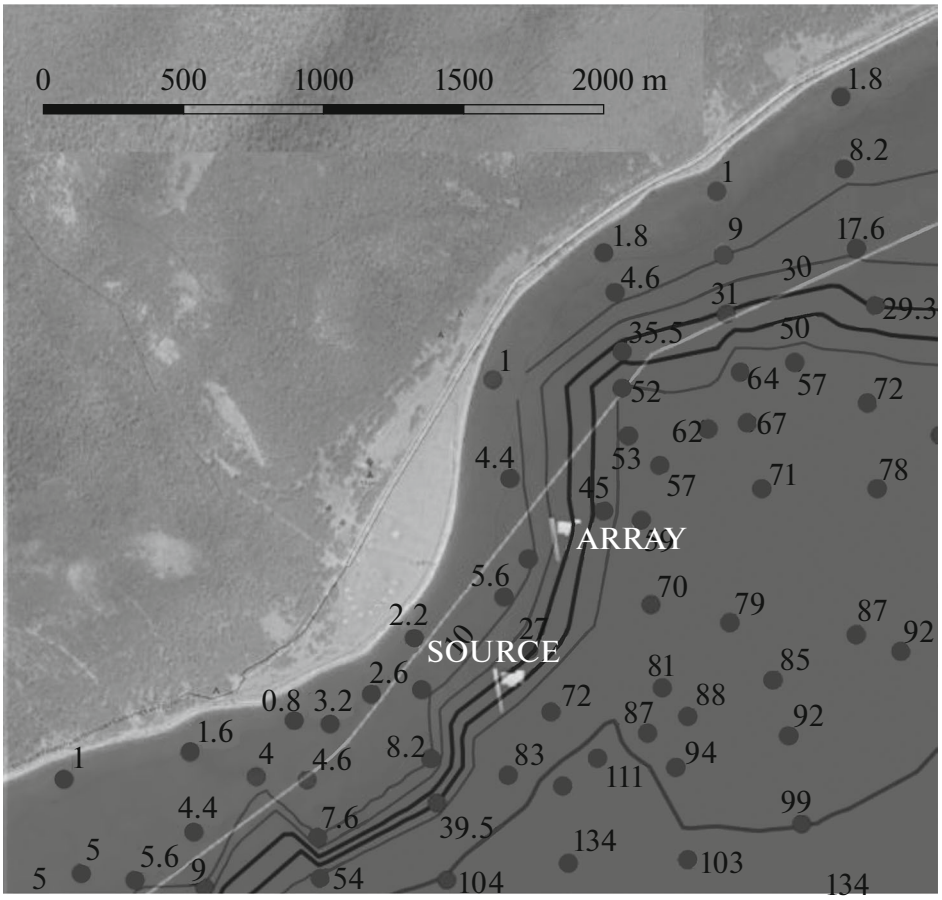

Fig. 2. Bathymetric map of the study area with locations of sound source and receiving array of hydrophones.

a comparison of the dependence of the experimentally obtained BER values on SNIR (average for the four signals) with the theoretical curve of dependence of BER on the signal-to-noise ratio (SNR) for a channel with interference in the form of additive white Gaussian noise (AWGN) in the absence of intersymbol interference [8].

The observed proximity of the experimental BER dependence on SNIR to the theoretical dependence for the AWGN channel itself does not make it possible to assume the similarity of the two channels, because the transmitted sequence was of random nature, and the intersymbol interference in this case appears for single receivers in the same way as additive noise. In order to separate the contribution of additive noise for each hydrophone from possible interference, a segment of the recording a few minutes before the communication sessions containing only background noise was considered. From this recording segment, SNR estimates were obtained using the following formula:

$$\mathrm{SNR} = 20\log_{10}\left(\frac{\sqrt{N}}{\sqrt{\sum_{n}\left|K_j w_j(n)\right|^2}}\right), \qquad (4)$$

where $N = 2000$ is the number of symbols in the transmitted binary sequence $s_0(n)$, $w_j(n)$ is the complex demodulated segment of the noise received on hydrophone number j and digitized with a frequency of one sample per symbol (analog of the signal $y_j(n)$ in formula (3)), and K_j is the normalization coefficient calculated for each hydrophone by formula (3).

Due to linearity of transformations, such processing results in decoding errors which would be introduced by additive noise into undistorted communication signal in case of its emission during the period of recording of this noise (i.e., "pure noise" SNR ratio). Listening to the recordings, visual analysis of their spectrograms, and analysis of the variability of the noise level outside the operating frequency band makes it possible to assume that the additive noise during the emission of communication signals differed from the considered noise segment of the recording insignificantly. Under this assumption, a comparison of the purely noise SNR values obtained for single hydrophones with the SNIR for communication signals (Fig. 4b) makes it possible to conclude that the contribution of additive noise to the overall interference dominated over intersymbol interference.

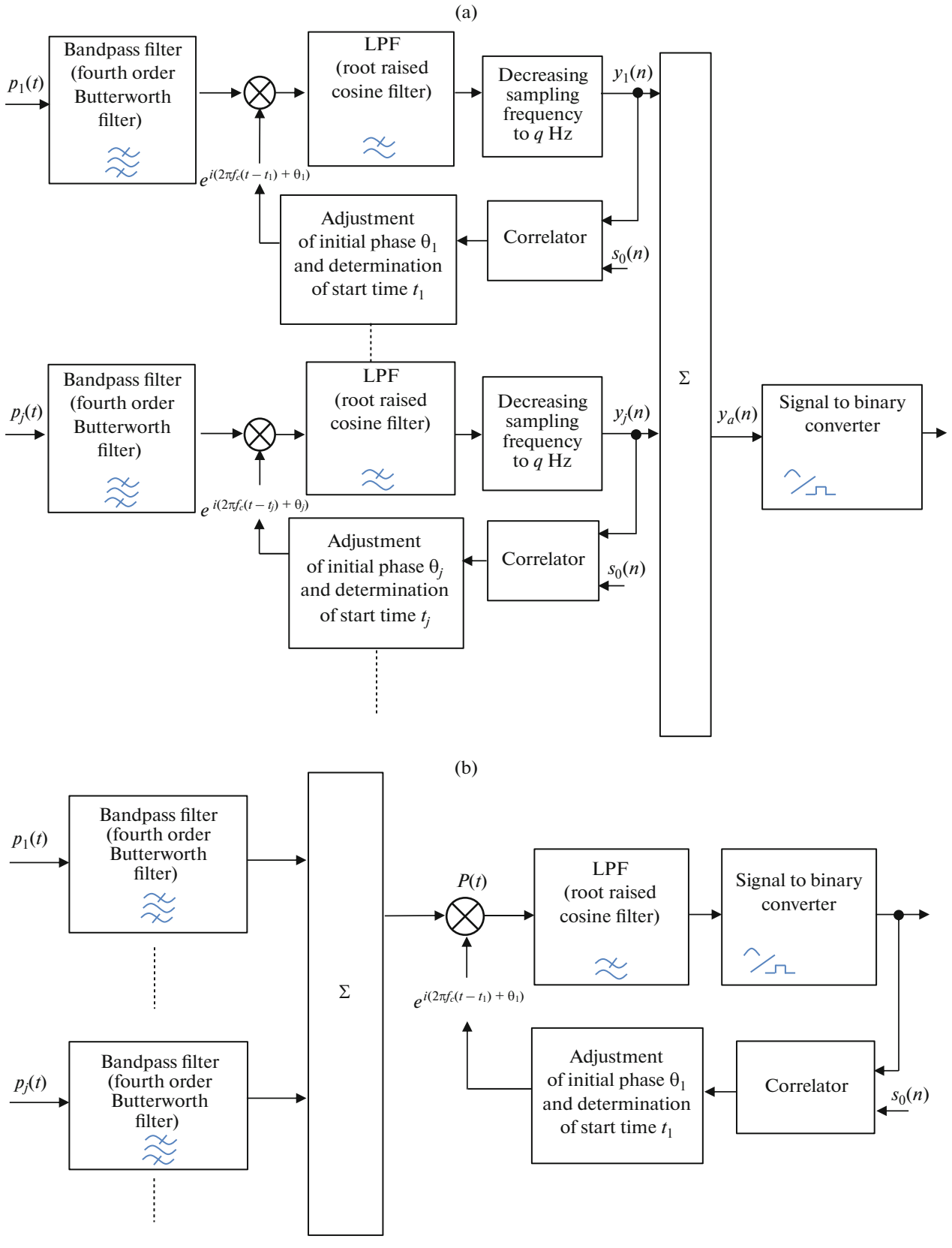

Fig. 3. Algorithm for processing signal from array: (a) with phase adjustment of signals from individual receivers, (b) without phase adjustment of signals from individual receivers, and (c) in case of passive time reversal procedure.

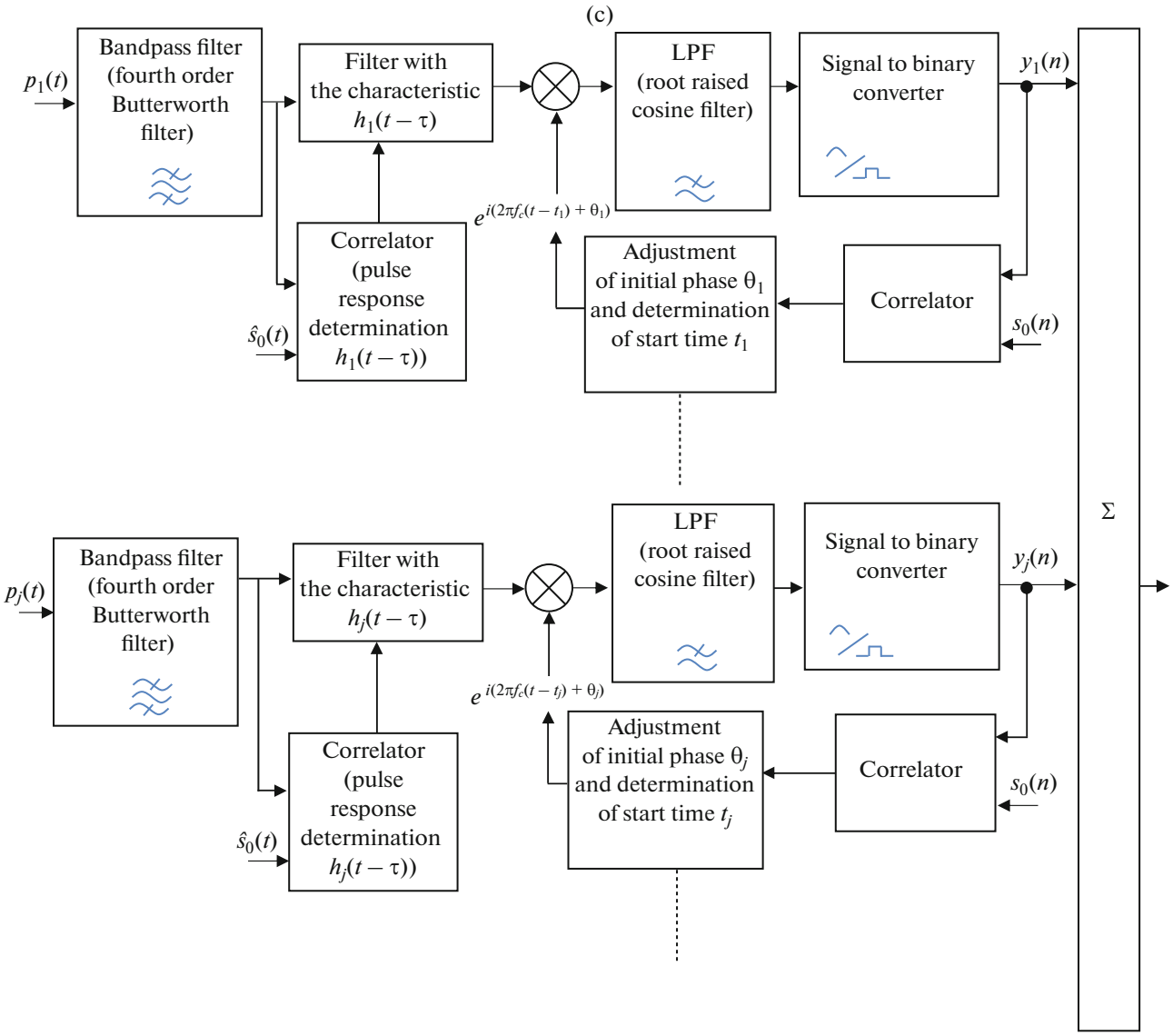

Fig. 3. (Contd.)

Table 1. Experimental values of BER and SNIR

Hydrophone number	Immersion depth, m	BER, % for one signal, average over four signals	BER, % for coherent sum of four signals	SNIR, dB for one signal, average over four signals	SNIR, dB for coherent sum of four signals
1	0.6	35.25	26.15	−12.7	−6.8
2	4.1	35.35	27.45	−13.7	−7.9
3	7.6	29.00	18.40	−9.5	−3.4
4	11.0	40.55	34.65	−17.5	−11.5
5	14.5	39.75	35.30	−17.3	−11.4
6	17.9	40.85	34.00	−16.7	−10.7
7	21.4	33.10	24.20	−12.3	−6.5
8	24.9	32.90	21.85	−11.3	−5.4
9	28.3	40.10	34.90	−17	−11.1
10	31.9	42.15	36.80	−18	−11.8

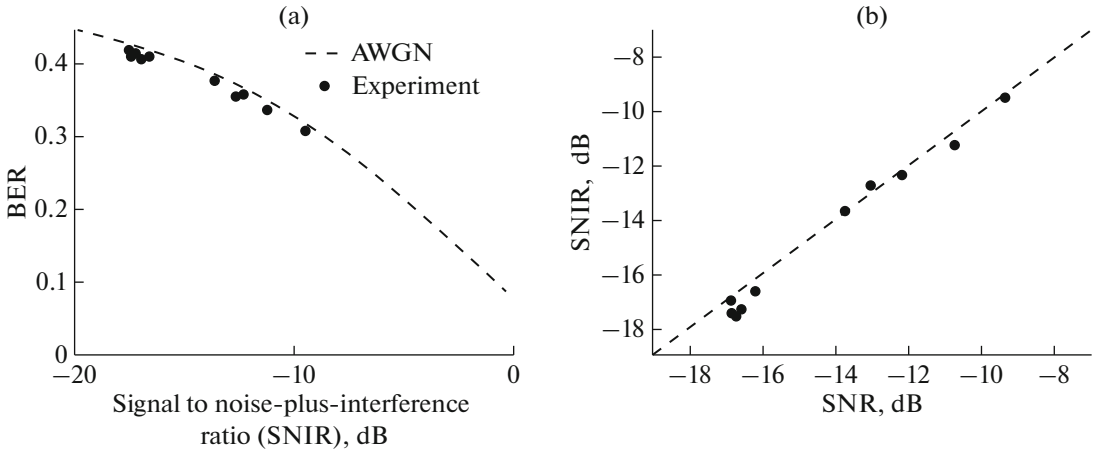

Fig. 4. Ratio of different types of interference and their combined effect on UAC quality. (a) Dependence of BER on level of signal to noise-plus-interference ratio (SNIR) in the experiment (points, average level over four signals for ten single receivers) and theoretical dependence of BER on the signal-to-noise ratio (SNR) for the channel with interference in form of additive white Gaussian noise (dashed line); (b) comparison of SNIR level in experiment (along the vertical axis) with SNR level for interference in form of additive noise recorded in absence of coherent signal (along horizontal axis).

However, note that, in general, the additive noise in the considered region was a nonstationary random process. Figure 5 shows an example of a segment of background noise recording containing short-term pulses of high intensity. The duration of one noise pulse is approximately 1 ms, and its amplitude exceeds the background level by 40–50 dB (Fig. 5b). The spectrum of such a pulse overlaps the range from several tens of hertz to several kilohertz (Fig. 5c). The emergence of this crackling is associated with changes in ambient temperature, e.g., in the morning after sunrise, when the ice begins to melt. Such a pulse interference can completely overlap several transmitted symbols, which can no longer be decoded. We should also note here that judging from the literature there is a general decrease in the average noise level under ice by 5–10 dB in comparison to the situation when there is no ice cover [13]. However, this advantage is not always implemented, and near the shore it is significantly determined by the level of anthropogenic noises, the sources of which can also be on shore.

The predominance of additive noise contribution in the total noise makes it possible to predictably increase the SNIR by a simple coherent summation of soft solutions for individual signals and hydrophones. Table 1 shows the results of such coherent summation over the four communication signals for each hydrophone. The decoding error suppression for all hydrophones is nearly identical to the theoretical $10\log_{10}4 = 6$ dB improvement that would be achieved in the case of no interference due to the simultaneous averaging of uncorrelated additive noise and signal power conservation.

In the observed case of background noise dominant over interference, coherent summation of signals over the array using the algorithm presented in Fig. 3a was expected to be close in efficiency to the coherent summation of the signals for the individual hydrophones of the array. For each of the four signals, addition over ten hydrophones increased SNIR by 9.8–10.2 dB. For a complete coherent sum over four signals and ten hydrophones, i.e., using a chain of hydrophones as a receiving uniform array, SNIR was 0.3 dB, improving the communication quality by 15.7 dB relative to the average error for single hydrophone reception. This improvement is clearly demonstrated by the soft decoding solutions shown in Fig. 6, i.e., in-phase and quadrature signal components[2] $y_j(n)$ and $y_a(n)$. (In this figure, the black dots correspond to the transmitted symbol −1 and the red ones to +1). Therefore, despite the significant communication quality advantage provided by the receiving uniform array, no additional improvement in UAC due to suppression of intersymbol interference is observed. Under the conditions of the described experiment, its contribution to the total error was insignificant compared to the influence of additive noise. The BER value for the total sum (for the array) was 4.9%.

In the case of the use of the algorithm shown in Fig. 3b, the BER for the same total component was 25.8%. In the case of using the passive time reversal (Fig. 3c), the BER was 9.2%. Therefore, the vertical array used in the experiment for all three algorithms improves the quality of data transmission; at the same time, the algorithm shown in Fig. 3a showed the best results.

NUMERICAL SIMULATION. INTERPRETATION OF THE EXPERIMENTAL RESULTS

In order to simulate UAC between a point source and a vertical discrete linear array, the technique described in [2] was used. Recall here the basic computational

[2] $y_a(n)$ is the signal received at the array output (see Fig. 3a).

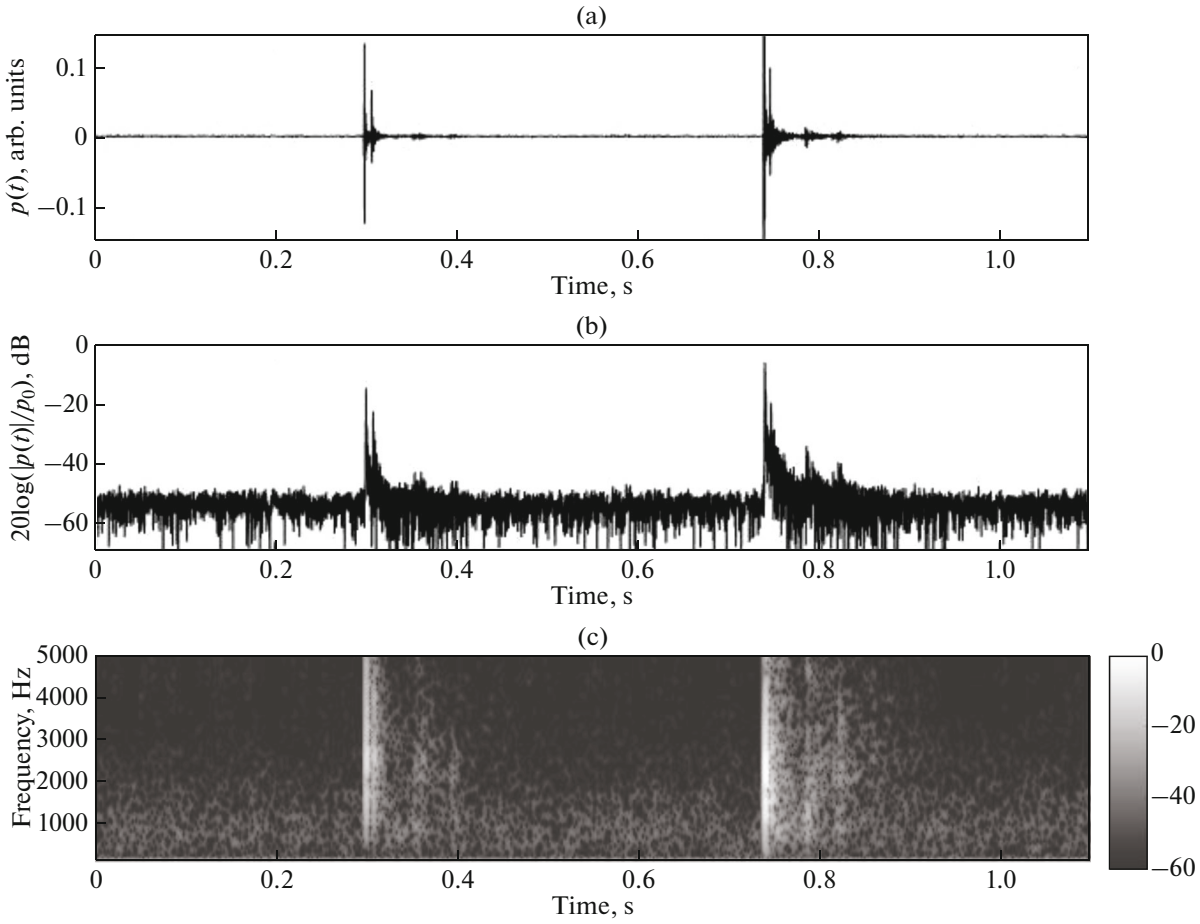

Fig. 5. Example of high-intensity pulse noise: (a) the received acoustic pressure $p(t)$ for time interval during which two episodes of pulse interference were recorded (at times ~0.3 and ~0.72 s), (b) level $p(t)$ in logarithmic scale, and (c) signal spectrogram. Signal was recorded by fourth hydrophone of array.

relationships for this technique, which is based on a mode description of the sound field [6]. The transfer function $K(\omega, r, z_0, z_j)$ between a point source and a hydrophone j at the receiver array is as follows[3]:

$$K(\omega, r, z_0, z_j) = NG(\omega, r, z_0, z_j),$$
$$G(\omega, r, z_0, z_j) = \sum_{m=1}^{M} \frac{\psi_m(z_0, \omega)\psi_m(z_j, \omega)}{\sqrt{q_m(\omega)r}} \exp\left(i\xi_m(\omega)r\right), \quad (5)$$

where N is the normalization factor of the length dimension and selected so that at a distance of 1 m there is a given level of acoustic signal emission, ω is the frequency, $G(\omega, r, z_0, z_j)$ is the Green's function for the Helmholtz equation with a point source function (delta function) in the right side, $\psi_m(z, \omega)$ and $\xi_m(\omega) = q_m(\omega) + i\,\gamma_m(\omega)/2$ are eigenfunctions (waveguide modes) and eigenvalues of the Sturm–Liouville problem for the waveguide under consideration. In the selected definition, the value $K(\omega, r, z_0, z_j)$ is a dimensionless quantity and determines the relationship between the spectra of emitted $\hat{S}_0(\omega)$ and received $P(\omega, r, z_0, z_j)$ signals: $P(\omega, r, z_0, z_j) = K(\omega, r, z_0, z_j)\hat{S}_0(\omega)$. In numerical simulations, it is more convenient to work in the time domain using the pulse characteristics of the $\hat{h}_j(t)$ channel:

$$\hat{h}_j(t) = \mathbf{F}^{-1}[K(\omega, r, z_0, z_j)]$$
$$\equiv \frac{1}{\pi}\mathrm{Re}\left[\int_{\omega_1}^{\omega_2} K(\omega, r, z_0, z_j)e^{-i\omega t}d\omega\right], \quad (6)$$

where $\Delta\omega = \omega_2 - \omega_1$ is the operating band of the signal, $\mathbf{F}^{-1}$ is the inverse Fourier transform operator, and **Re** is the real part. Then for the received signal $p_j(t)$ we can use the following convolution operation:

$$p_j(t) = \int_0^t \hat{s}_0(\tau)\hat{h}_j(t-\tau)d\tau, \quad (7)$$

where $\hat{s}_0(\tau) = \mathbf{F}^{-1}\left[\hat{S}_0(\omega)\right]$.

[3] Here, it is assumed that the waveguide parameters do not depend on distance r.

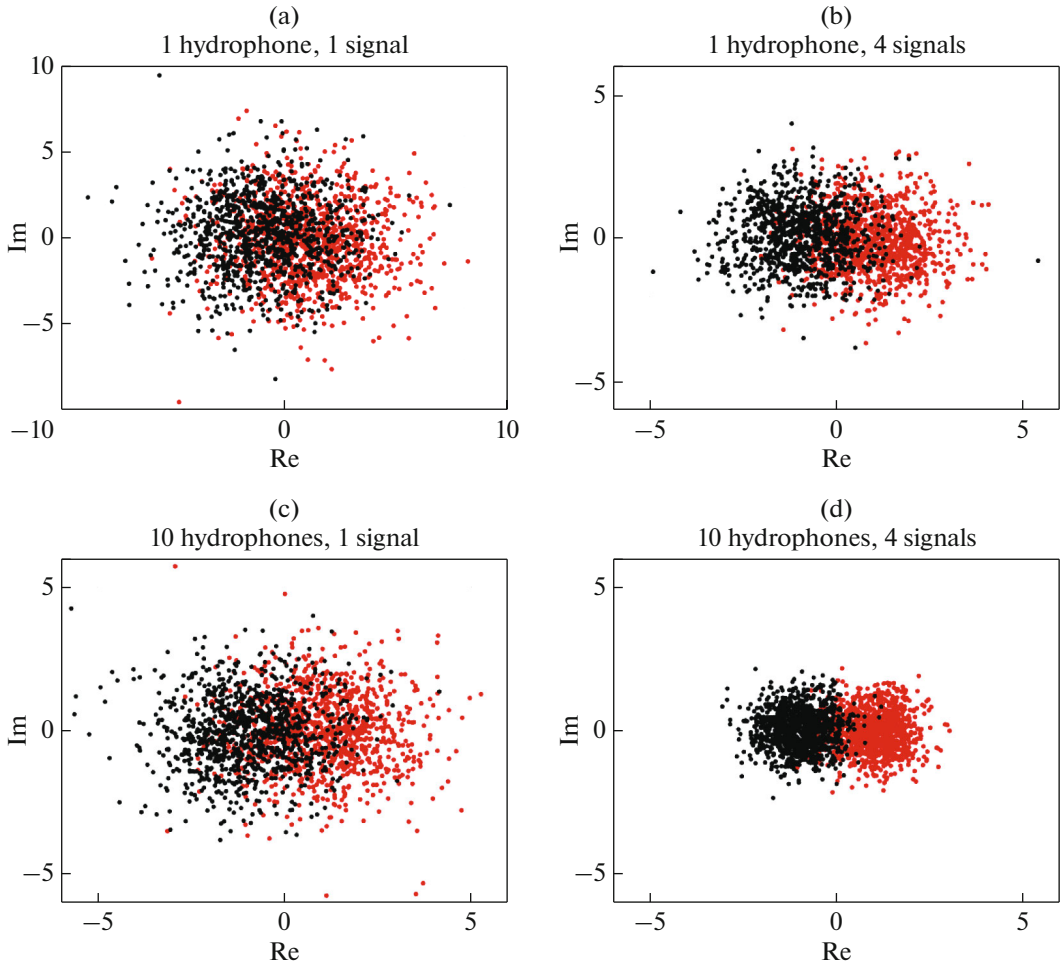

Fig. 6. Soft output (in-phase and quadrature components): (a) for one single receiver and one signal, (b) with coherent summation over four signals for one receiver, (c) with coherent summation over ten receivers for one signal, and (d) with coherent summation over all ten receivers and four signals.

For calculations of the function $G(\omega, r, z_0, z_j)$ in presence of ice cover, we used methodology described in [3]. In this case, the waveguide characteristics were selected to be close to the experimental ones. In particular, the waveguide depth was assumed constant and was $H = 48$ m, sound speed in water was $c = 1409$ m/s, and ice cover thickness was $h = 0.66$ m. The acoustic characteristics of the ice were selected as in [4]: longitudinal wave speed $c_2 = 3500$ m/s, transverse wave speed $c_s = 1800$ m/s, ice density $\rho_2 = 917$ kg/m^3, longitudinal wave attenuation factor $\beta_{2f} = 0.086$ dB/km/Hz, and transverse wave attenuation factor $\beta_{sf} = 0.556$ dB/km/Hz. The source depth was $z_0 = 18.44$ m. The bottom parameters determined by a special technique [3] were: bottom sound speed, $c_1 = 1670$ m/s, density, $\rho_1 = 1500$ kg/m^3, and bottom attenuation coefficient, $\beta_f = 0.45$ dB/km/Hz. It should be emphasized that all energy-carrying modes, including leaky modes and quasi-modes, were taken into account in the calculations.

The same emitted signal $\hat{s}_0(t)$ as in the above experiment was used for the simulation. The received calculated signal $p(t)$ was processed using the algorithms shown in Figs. 3a–3c. The simulation results (BER values) for different data rates are shown in Figs. 7–10. Noise was not considered here, and the only type of interference was the intersymbol interference. The results are presented for distances r between the sound source and receivers from 100 to 2000 m. As can be seen in the figures (see Figs. 8–10 vs. Fig. 7 (single receiver)), the numerical simulation also shows a significant improvement in communication quality when vertical linear arrays are used if there is no noise. Comparison of Fig. 7 with the results given in Table 1 once again confirms the conclusion that in the experiment the main errors in UAC were related to noise. They resulted in experimental BER values that were significantly higher than those in the simulation.

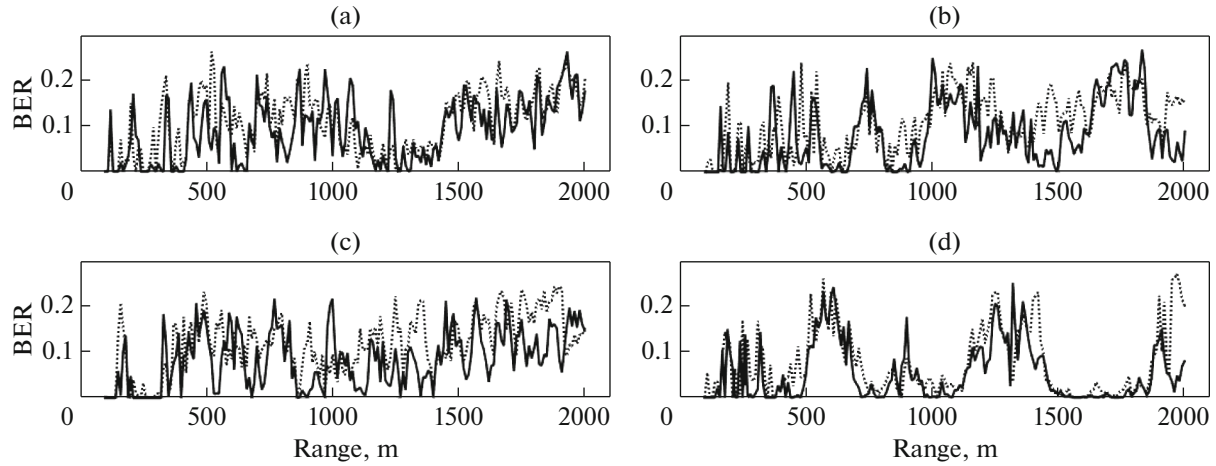

Fig. 7. Dependence of BER on range to sound source for single receiver at different depths: (a) receiving depth of 0.64 m, (b) receiving depth of 17.9 m, and (c) receiving depth of 24.9 m, and (d) receiving depth of 31.9 m. Solid line corresponds to transmission rate of 122.5 bps and dotted line, 183.75 bps.

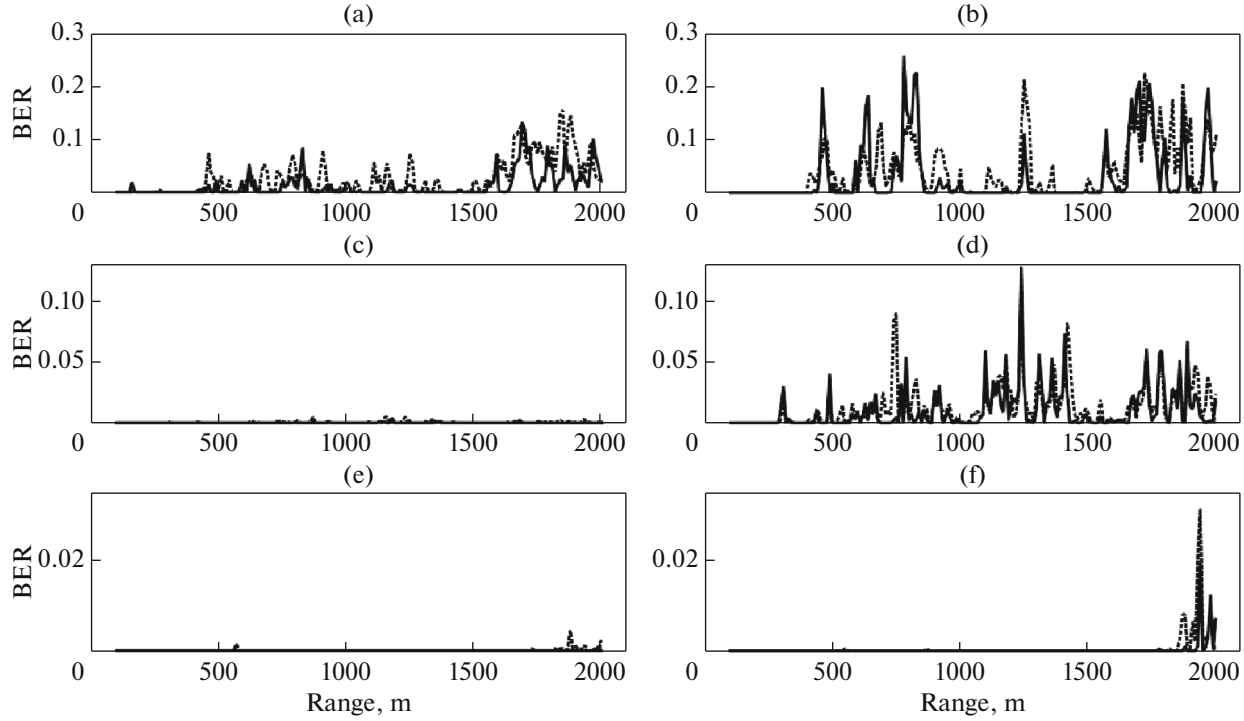

Fig. 8. Dependence of BER on range to sound source. Left row of figures was obtained using algorithm presented in Fig. 3a, right row was obtained using algorithm from Fig. 3b. solid line corresponds to data rate of 122.5 bps and dotted line, to 183.75 bps. Location of receivers: (a, b) five receivers at depths z_j = 22, 23, 24, 25, 26 m, (c, d) five receivers at depths z_j = 1, 10, 20, 30, 40 m, and (e, f) ten receivers at depths defined by formula (1).

The improvement in communication quality depends on both the array aperture length and the number of receivers. The range of acceptable BER values depends on the specifics of a particular problem, but conventionally it can be assumed that with BER < 0.1, the quality of communication remains satisfactory. In this case, using error-correcting codes [12], we can achieve error-free transmission of data while preserving an acceptable level of payload data in the transmitted signal. Calculations showed if there is no noise with any of the above spatial signal processing algorithms, this coefficient is obviously less than 0.1 in the case when the array overlaps more than half the thickness of the under-ice water layer, and the distance

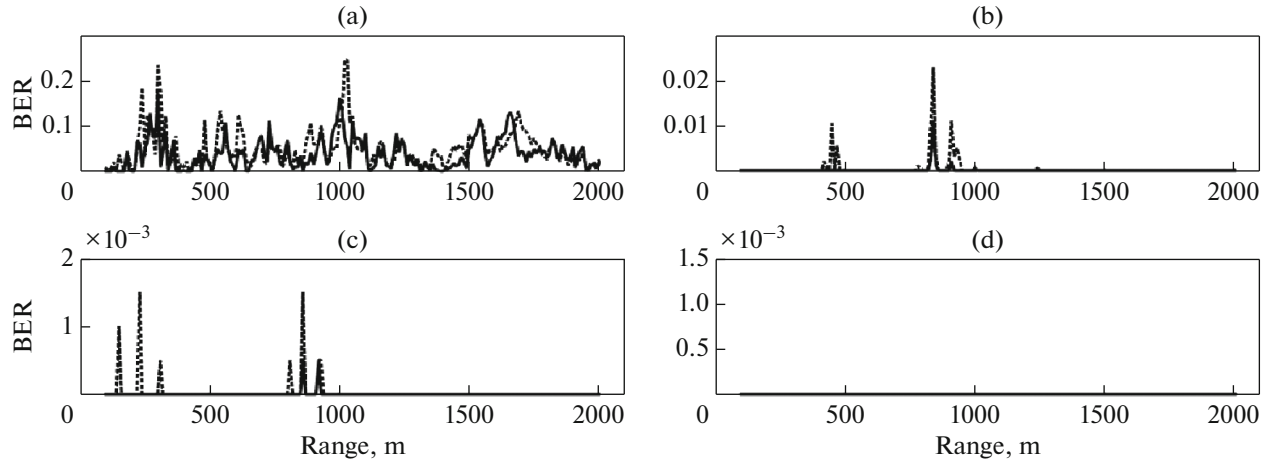

Fig. 9. Dependence of BER on range to sound source in case of passive time reversal application (see Fig. 3c). solid line represents 122.5 bps and dotted line, 183.75 bps. Location of receivers: (a) single receiver at a depth of 17.9 m, (b) five receivers at depths z_j = 22, 23, 24, 25, 26 m, (c) five receivers at depths z_j = 1, 10, 20, 30, 40 m, and (d) ten receivers at depths defined by formula (1).

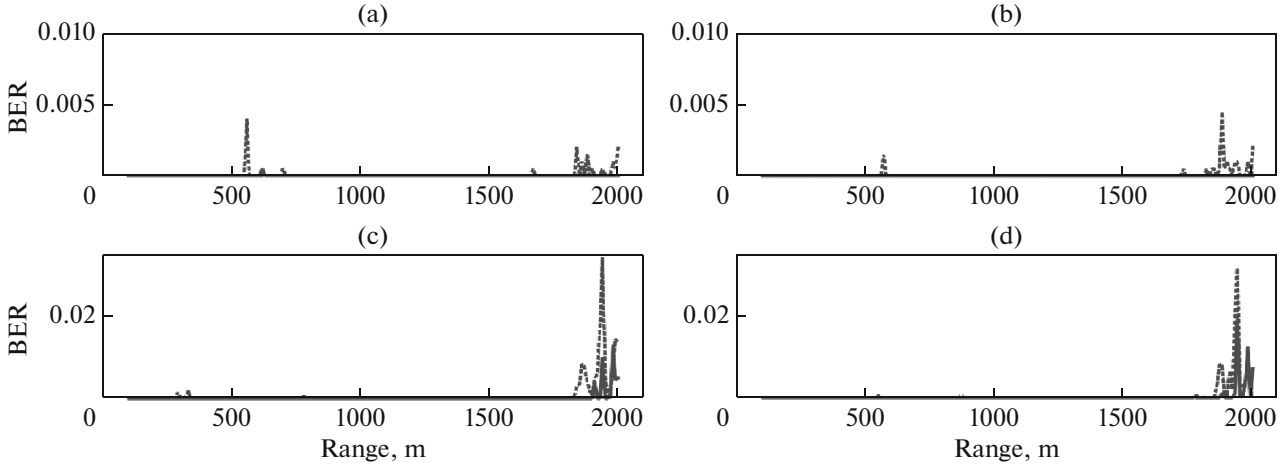

Fig. 10. BER estimates using mode selection (left) and without it (right): (a, b) results of algorithm shown on Fig. 3a and (c, d) algorithm from Fig. 3b. Solid line corresponds to data rate of 122.5 bps, and dotted line, to 183.75 bps.

between hydrophones is not greater than 2λ. If there is no noise, the best results are obtained when the algorithm based on the passive time reversal procedure is used (see Fig. 3c).

Here, it should also be emphasized that the tested algorithms (see Fig. 3a and 3b) did not use the mode selection of signals in oceanic waveguides proposed in [2, 8]. The attempt to apply one of the variants of mode selection [2] in simulation did not improve the UAC quality even when there was no noise (see Fig. 10). Processing of the experimental data led to the same result. Note that in numerical and field experiments the signals from the receiving hydrophones were multiplied by the value of the first waveguide mode at the depth of their installation (see formula (1)). Apparently, the inefficiency of the mode selection in the considered case was caused by the following factors. The distances between hydrophones l were significantly greater than $\lambda/2$. This led to the fact that the value of l exceeded the characteristic spatial period of vertical change for higher waveguide modes forming the sound field at the considered distances from the source. There were 35 of such energy-carrying modes. Therefore, here the UAC application conditions were fundamentally different from those considered, e.g., in [8], where l was comparable with $\lambda/2$, and relatively large distances were considered. Accordingly, only the modes of the first numbers with a large spatial variation period were energy-carrying in this work. It was for this situation that mode selection proved to be very effective.

CONCLUSIONS

In conclusion, note that the use of vertical linear arrays for the UAC essentially represents only the first

stage of processing of the received hydroacoustic signals. This stage does not preclude the application of other well-known adaptive equalization methods at the array output if necessary [7, 11, 12, 16], but it significantly reduces the requirements for these methods.

ACKNOWLEDGMENTS

We thank K.M. Kucher and M.M. Makarov for their assistance in conducting the experiments.

FUNDING

The study was supported by the Russian Foundation for Basic Research, project no. 19-02-00127, and by IO RAS, project no. 0128-2021-0010.

REFERENCES

1. R. A. Balakin and G. I. Vilkov, "Adaptation of a hydroacoustic communication channel with OFDM technology to the negative influence of a drifting ice cover," Acoust. Phys. **65**, 208–215 (2019).
2. M. V. Volkov, V. A. Grigoriev, A. A. Lunkov, and V. G. Petnikov, "On the possibility of using vertical receiving arrays for underwater acoustic communication on the Arctic shelf," Acoust. Phys. **65**, 269–278 (2019).
3. V. A. Grigoriev, K. M. Kucher, A. A. Lunkov, et al., "Acoustic parameters of the bottom in Lake Baikal," Acoust. Phys. **66**, 508–516 (2020).
4. J. M. Collis, S. D. Fran, A. M. Metzler, and K. S. Preston, "Elastic parabolic equation and normal mode solutions for seismo-acoustic propagation in underwater environments with ice covers," J. Acoust. Soc. Am. **139** (5), 2672–682 (2016).
5. L. Freitag, P. Koski, S. Singh, et al., "Acoustic communications under shallow shore-fast Arctic ice," in *Proceedings of the IEEE OCEANS'2017 Conf., Anchorage* (Curran Assoc., Red Hook, NY, 2017), pp. 1–5.
6. B. Katsnelson, J. Lynch, and V. Petnikov, *Fundamentals of Shallow Water Acoustics* (Springer-Verlag, New York, 2012).
7. D. B. Kilfoyle and A. B. Baggeroer, "The state of the art in underwater acoustic telemetry," IEEE J. Ocean. Eng. **25** (1), 4–27 (2000).
8. A. K. Morozov, J. C. Preisig, and J. C. Papp, "Investigation of mode filtering as a preprocessing method for shallow-water acoustic communications," IEEE J. Ocean. Eng. **35** (4), 744–755 (2010).
9. National Snow & Ice Data Center. http://nsidc.org/data/g01360.
10. A. J. Plueddemann, A. L. Kukulya, R. Stokey, and L. Freitag, "Autonomous underwater vehicle operations beneath coastal sea ice," IEEE/ASME Trans. Mechatron. **17** (1), 54–64 (2012).
11. J. C. Preisig, "Performance analysis of adaptive equalization for coherent acoustic communications in the time-varying ocean environment," J. Acoust. Soc. Am. **118** (1), 263–278 (2005).
12. J. Proakis, *Digital Communications* (McGraw-Hill, New York, 2001).
13. E. H. Roth, J. A. Hildebrand, S. M. Wiggins, and D. Ross, "Underwater ambient noise on the Chukchi Sea continental slope," J. Acoust. Soc. Am. **131** (1), 104–110 (2012).
14. D. Rouseff, "Counterintuitive results in underwater acoustic communications," in *Underwater Acoustics and Ocean Dynamics*, Ed. by L. Zhou, W. Xu, Q. Cheng, and H. Zhao (Springer-Verlag, Singapore, 2016), pp. 11–18.
15. D. Rouseff, D. R. Jackson, W. L. J. Fox, et al., "Underwater acoustic communication by passive-phase conjugation: theory and experimental results," IEEE J. Ocean. Eng. **26** (4), 821–831 (2001).
16. M. Stojanovic, J. G. Proakis, and J. A. Catipovic, "Performance of high rate adaptive equalization on a shallow water acoustic channel," J. Acoust. Soc. Am. **100** (4), 2213–2219 (1996).

Translated by O. Pismenov